Low-temperature polymorphs of ZrO$_2$ and HfO$_2$: A density-functional theory study

John E. Jaffe,[1] Rafał A. Bachorz,[1] and Maciej Gutowski[1,2,*]

[1]*Chemical Sciences Division, Fundamental Sciences Directorate, Pacific Northwest National Laboratory, P.O. Box 999,
Richland, Washington 99352, USA*

[2]*Department of Chemistry, University of Gdansk, 80-952 Gdansk, Poland*

The total energy and equation of state of the monoclinic, tetragonal, cubic, orthorhombic-I (*Pbca*) and orthorhombic-II (cotunnite) phases of zirconia and hafnia are determined using density functional theory (DFT) in the local density (LDA) and generalized-gradient (GGA) approximations. It is found that GGA corrections are needed to obtain low-temperature phase transitions under pressure that are consistent with experiment, i.e., (monoclinic→orthorhombic-I→cotunnite). The GGA values of the bulk modulus of the cotunnite phase are found to be 251 and 259 GPa for ZrO$_2$ and HfO$_2$ respectively, highlighting the similarity of these two compounds. We introduce a population analysis scheme in which atomic radii are adapted to the actual charge distribution in the material. The results indicate that the effective atomic radius of Hf is smaller than that of Zr, a drastic manifestation of the relativistic lanthanide contraction. The population analysis demonstrates that ionicity: (i) decreases from the monoclinic to the cotunnite phase, and (ii) is larger for HfO$_2$ than for ZrO$_2$. The bandgap and heat of formation are also larger for monoclinic HfO$_2$ than for ZrO$_2$ by 0.60 eV and 0.60 eV/ formula unit, respectively. The tetragonal phase, which often exists as a metastable phase at ambient conditions, has a bandgap larger than the monoclinic phase by 0.35 and 0.65 eV for ZrO$_2$ and HfO$_2$, respectively.

PACS number(s): 64.70.Kb, 64.30.+t, 77.84.Bw

I. INTRODUCTION

Among refractory transition metal compounds, ZrO$_2$ and HfO$_2$ have attracted exceptional research interest in recent years, from both fundamental and technological perspectives. In various forms and sometimes with the addition of small amounts of other oxides, they have applications ranging from solid oxide fuel cell electrolytes and microelectronic gate dielectrics[1–3] to catalyst substrates, protective coatings, and synthetic gemstones. They also show a rich variety of crystal structures depending on pressure, temperature, impurity/dopant content, growth conditions, and epitaxial strain. Besides the well-known monoclinic, tetragonal, and (extrinsically stabilized) cubic phases, the orthorhombic high pressure phases with space group symmetry *Pbca* (orthorhombic-I) and *Pnma* (orthorhombic-II, also called PbCl$_2$ or cotunnite structure) have recently attracted the attention of researchers. The cotunnite phase in particular can be quenched to ambient conditions[4,5] and has been suggested as a candidate for a useful superhard material.[6] Unit cells of these structures are sketched in Figs. 1(a)–1(e).

It is known that the chemistries of hafnium and zirconium are more nearly identical than for any other two congeneric (same Periodic Table column) elements. This similarity is commonly attributed to the lanthanide contraction of Hf that is responsible for the similar atomic and ionic radii of Zr and Hf as well as their similar ionization potentials.[7] However, recent reports indicate small but technologically important differences between Zr and Hf compounds: (i) the HfO$_2$/Si interface has been found to be stable with respect to formation of silicides whereas the ZrO$_2$/Si interface is not;[1,3] (ii) significant differences in elastic behavior and transition pressures were suggested for ZrO$_2$ and HfO$_2$;[6] and (iii) the temperature-induced monoclinic to tetragonal transition in HfO$_2$ is about 500 K higher than in ZrO$_2$.[8]
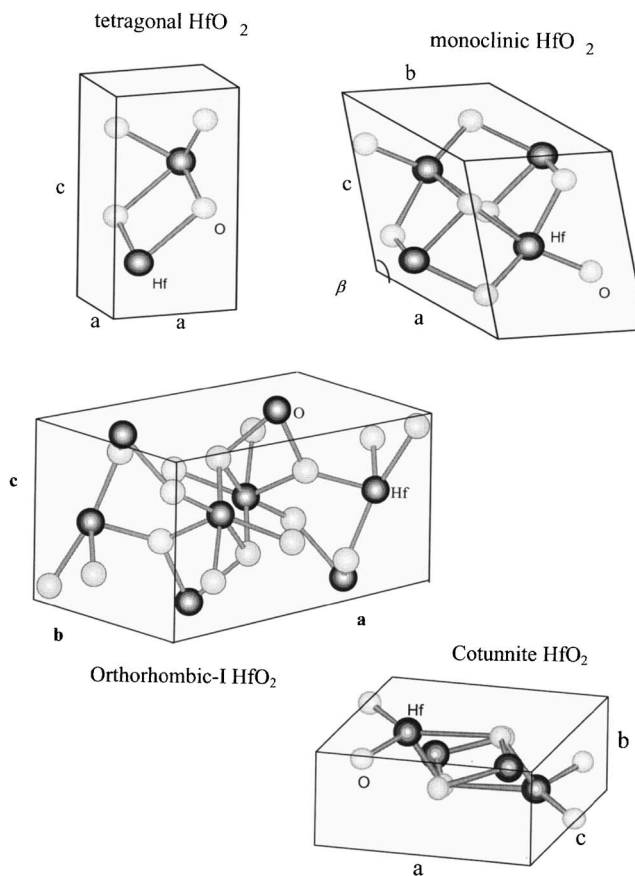
FIG. 1. The unit cells for the following structures of ZrO$_2$ and HfO$_2$, using HfO$_2$ as an example: monoclinic, orthorhombic-I, tetragonal, and cotunnite (orthorhombic-II).

Minority phases of ZrO_2 and HfO_2 that are useful for some purposes may be deleterious for others. Thin films in particular, such as might be used in CMOS gates, have been found to often contain both the monoclinic and metastable tetragonal phases.[9] If other metastable phases, like the cotunnite structure, are close in energy to the tetragonal phase, they could also occur in films of ZrO_2 or HfO_2. However, the high-pressure phases are also of higher density than the equilibrium phase, and if these dense phases in a film convert spontaneously to the majority low pressure phase, the resulting strain would disrupt or delaminate the film. Thus, it is desirable to be able to either promote or suppress the formation of metastable phases of HfO_2 and ZrO_2, depending on the intended application. A detailed knowledge of the energetics of all the relevant phases would be very useful for achieving practical control over the structure of these oxide films.

There are also questions of basic interest about the possible phases of these oxides, from both experimental and theoretical standpoints. We aim to confirm the exact sequence of equilibrium low-temperature phases as a function of pressure, whether it is the same for both ZrO_2 and HfO_2, and whether it has any universal features such as a relation between crystal ionicity, coordination, and valence electronic structure. In connection with the ionicity we introduce a method of electron population analysis based on atomic radii optimized to describe the pseudocharge density obtained in first-principles plane wave calculations. We also identify some small differences in phase stability between ZrO_2 and HfO_2. We note that a recent paper[10] studied the high-pressure phases of HfO_2 in detail, but a critical comparison with high-pressure ZrO_2 is also needed. Finally, we seek to clarify a prediction[11] that the cotunnite structure in ZrO_2 has a lower energy than the monoclinic baddeleyite structure, in disagreement with the experiment.

In Sec. II we describe details of our density functional theoretic computational procedure for predicting the low-temperature energetics of the various phases of these two oxides. Our main results are presented in Sec. III and compared with earlier computational studies and experiments, while Sec. IV is a summary.

II. COMPUTATIONAL TECHNIQUE

We used periodic density functional theory (DFT) within the generalized gradient approximation[12] (GGA) and, for comparison, the local density approximation (LDA) to perform structure optimizations and total energy calculations[13] on the five phases of HfO_2 and ZrO_2 mentioned above. We expanded the eigenstates in plane-wave basis functions, represented the ion cores with ultrasoft pseudopotentials,[14] and treated the Zr $4d$ and $5s$, Hf $5d$ and $6s$, and O $2p$ and $2s$ states as fully relaxed energy bands. Test calculations on cubic, tetragonal, and monoclinic ZrO_2 with the semicore $4p$ states also treated as valence bands revealed only minor changes in structural energy differences from those obtained with the Zr $4p$ states in the core. We optimized the atomic geometry with Hellman-Feynman forces and conjugate gradients.[15] High precision settings were used throughout to

TABLE I. The equilibrium structures (GGA). All angles are 90° except monoclinic β; the fractional coordinates are shown below the lattice constants.

Compound	Structure		a (Å)	b (Å)	c (Å)
ZrO_2	Monoclinic		5.1974	5.2798	5.3498
	β=99.53°	Zr	0.276	0.043	0.207
		O1	0.071	0.336	0.342
		O2	0.448	0.758	0.480
	Orthorhombic-I		10.1745	5.3148	5.1357
		Zr	0.885	0.035	0.253
		O1	0.790	0.375	0.127
		O2	0.977	0.739	0.497
	Tetragonal		3.6287		5.2070
		Zr			0.000
		O			0.210
	Cubic		5.1280		
	Cotunnite		5.6140	3.3474	6.5658
		Zr	0.246	0.250	0.113
		O1	0.360	0.250	0.425
		O2	0.024	0.750	0.338
HfO_2	Monoclinic		5.1284	5.1914	5.2969
	β=99.71°	Hf	0.277	0.043	0.209
		O1	0.074	0.342	0.337
		O2	0.448	0.759	0.481
	Orthorhombic-I		9.8323	5.1688	4.9617
		Hf	0.885	0.036	0.257
		O1	0.794	0.382	0.138
		O2	0.975	0.738	0.496
	Tetragonal		3.5775		5.1996
		Hf			0.000
		O			0.195
	Cubic		5.0628		
	Cotunnite		5.5530	3.3029	6.4842
		Hf	0.246	0.250	0.112
		O1	0.359	0.250	0.426
		O2	0.024	0.750	0.339

insure a well-converged calculation. In particular, we used a $9 \times 9 \times 9$ Monkhorst-Pack[16] net to sample the Brillouin zone (except $5 \times 7 \times 7$ in the orthorhombic-I structure) and a kinetic energy cutoff of 495 eV. Test calculations with a lower kinetic energy cutoff (396 eV) produced changes smaller than 5 meV per formula unit in total energies of individual phases of HfO_2, and changes in energy differences between phases of less than 3 meV, or about 1%. Hence, the plane-wave expansion is well converged.

Equations of state at $T=0$ for each phase were obtained by calculating the total energy at several (5–10) fixed values of the unit cell volume, fully minimizing the energy with respect to the c/a and b/a ratios (or monoclinic angle β in the case of the baddeleyite structure) and internal fractional coordinates at each volume. The total energy E of each phase (identical with the internal energy at $T=0$) as a function of

TABLE II. The equation of state parameters for ZrO$_2$ from the present work, earlier density-functional calculations, and the experiment. The coordination number of O atoms around the metal atom is given after the space group symbol.

ZrO$_2$			Present, LDA	Present, GGA	Other work, LDA	Experiment
Monoclinic		E_0 (eV)	0.000	0.000	0.000	0.000
$P2_1c$	7	V_0 (Å^3)	34.170	36.186	35.628[a], 34.158[b]	35.22[d], 35.16[f]
		B_0 (GPa)	184	137	157[a]	212[f]
Orthorhombic I		E_0 (eV)	0.014	0.049	−0.033[a]	
$Pbca$		V_0 (Å^3)	32.967	34.688	31.733[a]	33.49[f]
	8	B_0 (GPa)	236	204	272[a]	243[f]
Tetragonal		E_0 (eV)	0.038	0.109	0.057[b]	0.063[c]
$P4_2nmc$	8	V_0 (Å^3)	32.600	34.470	32.406[b]	33.67[d]
		B_0 (GPa)	225	199		
Cubic		E_0 (eV)	0.067	0.171	0.015[a], 0.102[b]	0.120[c]
$Fm3m$						
	8	V_0 (Å^3)	32.144	33.712	33.751[a], 31.906[b]	32.89[d]
		B_0 (GPa)	278	251	267[a]	
Cotunnite		E_0 (eV)	0.037	0.262	−0.025[a]	
$Pnma$	9	V_0 (Å^3)	29.241	30.859	29.414[a]	30.161[e], 30.805[f]
		B_0 (GPa)	298	251	305[a]	444[f]

[a]Reference 11
[b]Reference 23
[c]Reference 22
[d]Reference 18
[e]Reference 19
[f]Reference 20

volume V was then least-squares-fitted to the Murnaghan[17] equation of state, with dB/dp fixed to 4, to obtain a smooth function; in each case the fit to the three-parameter equation was excellent. Transition pressures were then extracted by a common tangent construction. The parametrized $E(V)$ equations of state were also transformed to enthalpy (identical with the Gibbs energy at $T=0$) vs pressure curves, for which the transition pressures are then simply given by the crossing points; this procedure gives physically equivalent results to the common tangent construction but is numerically more accurate.

Bonding in solids is often described in terms of concepts such as ionicity, covalency, or metallicity. Such a classification of solids, if derived from an electronic structure calculation, requires some form of electron density or "population" analysis, that is, a physically reasonable partition of electronic charge among the atoms in the system. When a plane-wave expansion is used, it is often convenient to simply integrate the charges within nucleus-centered spheres to obtain populations (and projected densities of states) but then the question arises of what radii to use. A popular strategy is to use some set of "touching" radii, such as a standard set of covalent radii, and then scale them so that the sum of sphere volumes equals the actual total volume of the unit cell. Such an approach does not in general keep the sum of all atomic charges equal to the exact charge of the unit cell, because of using possibly inappropriate radii as well as double-counting of electronic charges near the interatomic bonds, while neglecting some of the interstitial spaces. For many nonmetallic solids, the bonding is neither purely ionic nor covalent, but rather some mixture which we would like to determine from our calculation, rather than using a set of arbitrary radii valid only in the ionic or covalent limit.

Here, we propose a simple method to adapt the radii to the actual charge distribution in the material under study while maintaining the "volume sum rule" and minimizing the error in the total electronic charge. We search the space of sets of atomic radii consistent with the volume sum rule, and integrate the total charge within the spheres, taking care not to double-count the charge in the overlap regions. Since some interstitial charge is always neglected, the total we obtain is always less than the exact charge of the cell. We then maximize the integrated charge with respect to the atomic radii, subject to the volume constraint. We take the radii corresponding to this maximum as the appropriate set of atomic radii for the phase under consideration (all this being done at the unit cell geometry corresponding to the minimum energy for that phase). The electron density is integrated over volumes of the resulting individual spheres to provide an effective number of electrons per each atom. We also eliminate

TABLE III. The equation of state parameters for HfO_2 from the present work, earlier density-functional calculations, and the experiment. The notation is as in TABLE II.

HfO_2			Present, LDA	Present, GGA	Other work, LDA[a]	Other work, GGA[e]	Experiment
Monoclinic		E_0 (eV)	0.000	0.000	0.000		
$P2_1c$	7	V_0 (Å^3)	32.733	34.812	34.552	36.39	30.295[c], 34.665[d]
		B_0 (GPa)	215	152	251	192	284[c], 145[d]
Orthorhombic I	8	E_0 (eV)	0.029	0.065	0.020		
$Pbca$		V_0 (Å^3)	31.502	33.527	34.460	35.04	28.930[c], 33.105[d]
		B_0 (GPa)	240	197	256	221	281[c], 210[d]
Tetragonal		E_0 (eV)	0.099	0.156			
$P4_2nmc$	8	V_0 (Å^3)	31.272	33.297		34.82	
		B_0 (GPa)	219	201		183	
Cubic		E_0 (eV)	0.152	0.237	0.056		
$Fm3m$	8	V_0 (Å^3)	30.744	32.449	33.949	34.10	
		B_0 (GPa)	288	260	280	257	
Cotunnite		E_0 (eV)	0.167	0.385	0.020		
$Pnma$		V_0 (Å^3)	28.026	29.747	30.659	31.18	29.652[b], 26.54[c], 30.505[d]
		B_0 (GPa)	312	259	306	252	340[c], 475[d]

[a]Reference 11
[b]Reference 19
[c]Reference 20
[d]Reference 21
[e]Reference 10

double-counting of charge in the overlap zones in this stage of the analysis, but charge in the interstitial regions is not included, so these populations in general sum to a positive net charge in the unit cell when atomic core charges are counted. However, the undercounting of the total electron charge is fairly small, and the partial densities of states resulting from projection into these spheres add up rather closely to the total density of states.

The resulting radii are reasonable in that they are between typical ionic and covalent radii, but closer to the ionic radii, as we would expect for most metal oxides. We will see below that the radii shift towards less "ionic" values (smaller anion relative to the cation) when phases become more compressed. The charge counts inside individual spheres are also quite reasonable for semi-ionic oxides, with the nominally tetravalent metal atoms having charge between three and four, and show the proper physical trends (more polar charge distribution for more "ionic" radii). This population analysis allows quantifying differences between phases and between ZrO_2 and HfO_2.

III. RESULTS AND COMPARISONS

The values of equilibrium ($p=0$) lattice constants and nonredundant fractional coordinates are presented in Table I

and the Murnaghan equation of state parameters derived from our calculations are shown in Tables II (ZrO_2) and III (HfO_2), along with experimental data[18–22] and results from other computational works.[10,11,23] All extensive quantities are given per MO_2 formula unit. Theoretical total energies are all given relative to the monoclinic phase, which is experimentally the lowest energy phase of both compounds. The tables show that the GGA results are in better overall agreement with experiment, where the latter is available, than the LDA. This finding is in line with several computational studies[24] on phase transitions under pressure. We note that in addition to the theoretical works cited above, there have been several other first-principles calculations on zirconia[25–28] and hafnia[10,28–30] which we have not included in Tables I–III because either they did not consider the high pressure phases, or did not include total energy differences, bulk moduli, and transition pressures,[26,28,29] or because their results[27,30] for crystallographic parameters were extremely close to ours. We refer the reader directly to these studies for detailed comparisons.

For each phase, the volume per formula unit is smaller for HfO_2 than ZrO_2 as if the ionic radius was smaller for $Hf(+\delta)$ than for $Zr(+\delta)$. See also Fig. 2, in which we plot the total energy of each phase as a function of that phase's $p=0$ volume. The difference in V_0 is the largest for the orthorhombic-I structure (4.2 %) and the smallest for the te-
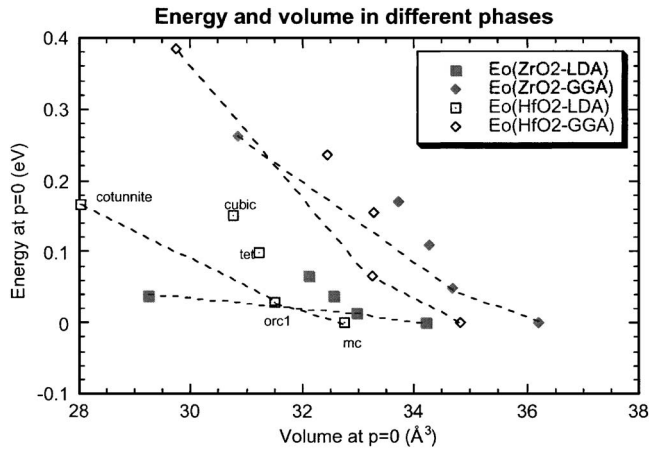
FIG. 2. The total energy at zero pressure versus volume at zero pressure for each phase of ZrO$_2$ and HfO$_2$ in the LDA and GGA. For each oxide and method the leftmost point corresponds to the cotunnite phase and is followed by the cubic, tetragonal ("tet"), orthorhombic-I ("orc1"), and monoclinic ("mc") phases. The dashed lines connect phases accessible at room temperature under compression (cotunnite, orthorhombic-I, and monoclinic).

tragonal structure (2.9 %). This result is surprising because usually for congeneric elements an increase in the atomic number leads to an increase of the atomic or ionic radius. For typical elements from the second and third transition metal rows such an increase is reduced by the lanthanide contraction, whereas for Zr and Hf the relative sizes are apparently reversed. Indeed, the recommended ionic radius for "Hf(+4)" is smaller by 0.01 Å than that for "Zr(+4),"[7] which qualitatively confirms our structural predictions.

Our results from Tables II and III demonstrate that the GGA value of bulk modulus for the monoclinic phase of HfO$_2$ is 152 GPa and is larger by 15 GPa than for ZrO$_2$. This difference is smaller, or even reversed, for other polymorphs. For both ZrO$_2$ and HfO$_2$ the orthorhombic-I and tetragonal forms are characterized by a similar value of bulk modulus as are the cubic and cotunnite phases. The LDA values of bulk modulus are systematically larger than the GGA values, possibly due to a smaller value of V_0 for the former functional.

The GGA values of bulk modulus for the cotunnite phase of ZrO$_2$ and HfO$_2$ are 251 and 259 GPa, respectively. Our results raise some concerns about whether cotunnite-phase ZrO$_2$ and HfO$_2$ are really "superhard." We consistently predict bulk moduli below 260 GPa as opposed to the values above 400 GPa reported from some experiments.[20,21] In particular, the molar volume reported for cotunnite HfO$_2$ in Ref. 20 appears to be too small, which would result in an overestimate of B_0.

Our results for the total energy as a function of volume are plotted in Figs. 3(a)–3(d) for ZrO$_2$ and HfO$_2$ in the LDA and GGA. A common tangent construction, as shown on the figures, determines the transition pressures between phases. While our LDA results for ZrO$_2$ do not show the spurious lowering of the energy of the cotunnite and orthorhombic-I structures below that of the monoclinic phase,[11] we do find a more subtle disagreement with experiment. There is no transition to the orthorhombic-I phase, because the transition to cotunnite (orthorhombic-II) occurs first. This indicates that the LDA energy for the cotunnite phase is still too low, while the GGA rectifies that problem.

From the computed equation of state parameters we also calculated the enthalpy[31] $H(p) = E + pV$ as a function of pressure for all the phases of the two compounds under consideration in the LDA and GGA. Transition pressures were taken from the curve crossings, i.e., those pressures where the enthalpies of two phases coincide, and no phase has a lower enthalpy. In Table IV we compare these pressures to the experimental pressures[20,21,32,33] at which the transitions to the orthorhombic phases were observed under conditions of increasing pressure. Our GGA transition pressures and those of Ref. 10 for HfO$_2$ are in reasonable agreement with some measurements,[32,33] but lower than others.[20,21] However, the

TABLE IV. The transition pressures p_{t1} from a monoclinic to an orthorhombic-I structure, p_{t2} from an orthorhombic-I to a cotunnite structure, or p_t from the monoclinic structure directly to the cotunnite structure.

	Present LDA	Present GGA	Ref. 11 LDA	Ref. 10 GGA	Experiment
ZrO$_2$					
p_{t1} (GPa)		6.64	−1.54		10[a], 3–4[c]
p_{t2} (GPa)		9.20	−0.36		25[a], 12.5[c]
p_t (GPa)	1.20				
HfO$_2$					
p_{t1} (GPa)	4.13	7.79		3.8	10.0[a], 10[b], 4[c] 4.3[d]
p_{t2} (GPa)	6.50	15.30		10.6	32[a], 27[b], 14.5[c], 12[d]
p_t (GPa)			0.53		

[a]Reference 20
[b]Reference 21
[c]Reference 32
[d]Reference 33
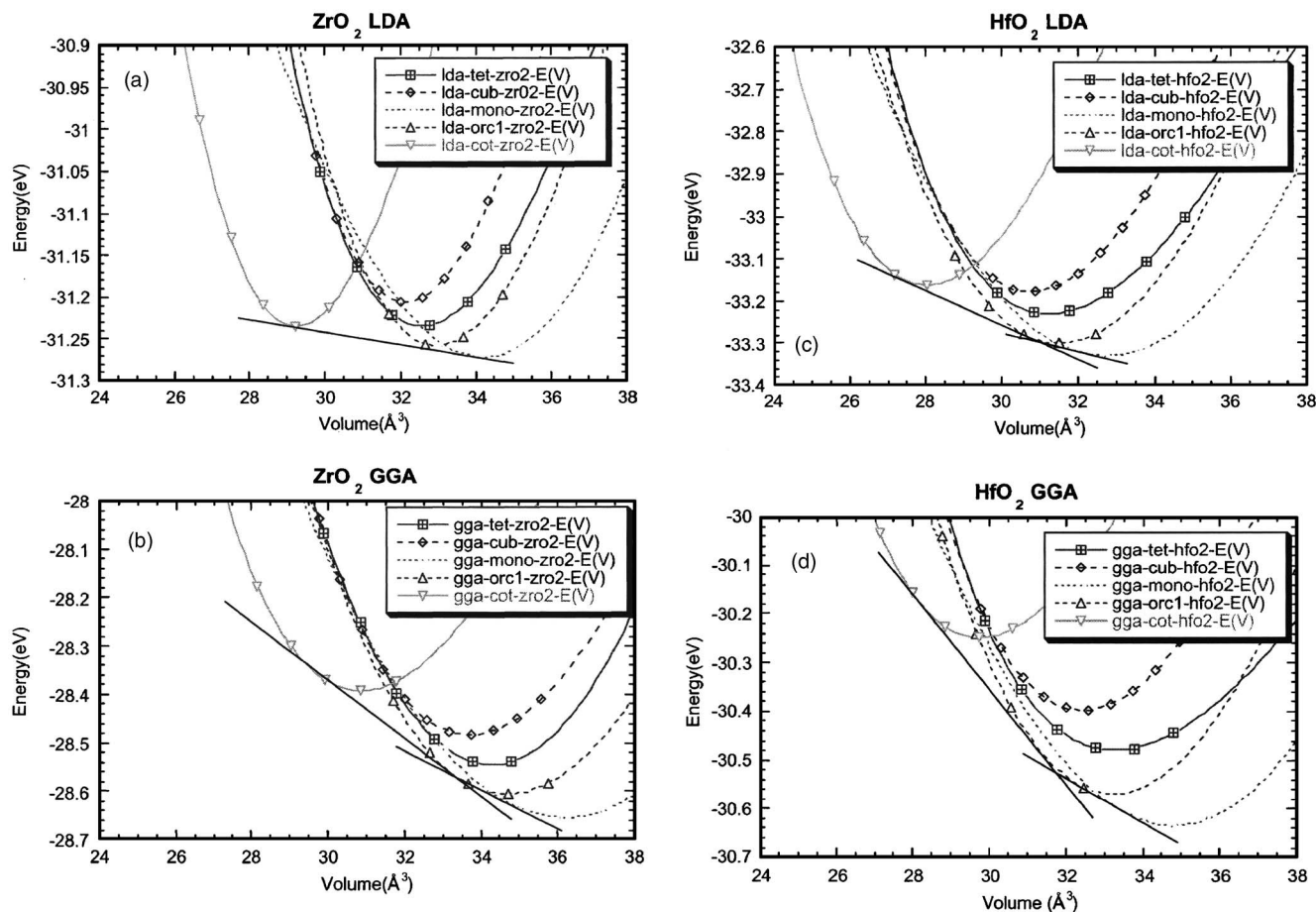
FIG. 3. The computed total energy versus volume in the five structures of Fig. 1, for: (a) ZrO_2, LDA; (b) ZrO_2, GGA; (c) HfO_2, LDA; (d) HfO_2, GGA. Here cot=cotunnite, orc1=orthorhombic-I, cub=cubic, tet=tetragonal, and mono=monoclinic.

computed values are *equilibrium* transition pressures, while the experiments tend to show a large amount of hysteresis. The high-pressure phases can be quenched to lower pressure (to ambient in the case of cotunnite) so it is reasonable to assume that the low-pressure structures likewise persist beyond the equilibrium transition when the pressure is initially applied. In consequence, the computed transition pressures would only be lower limits to the transition pressures observed under conditions of increasing pressure, so that some of the measured pressures are higher, as seen in Table IV.

The negative transition pressures deduced from Fig. 2 of Ref. 11 for ZrO_2 reflect excessively low energies for both high-pressure phases, while the direct transition[11] to the cotunnite phase in HfO_2 reflects a too-low energy for that phase also. Besides the neglect of gradient corrections in the LDA, these inaccuracies in Ref. 11 may come from their choice of pseudopotentials, especially for oxygen. The transition pressures for HfO_2 found in Ref. 10 with the GGA are in fair agreement with ours, being somewhat closer to our LDA than to our GGA values, and somewhat further from the majority of experimental results than our GGA values are.

The monoclinic and tetragonal phases are the most common in thin films of zirconia and hafnia.[9] Our results indicate that these two phases are separated by 0.11 and 0.16 eV for ZrO_2 and HfO_2, respectively. This is in qualitative agreement with experimental findings that the monoclinic to tetragonal transition in HfO_2 is about 500 K higher than in ZrO_2.[8]

The substantial hardness of the cotunnite phase and its stability under ambient conditions deserves further investigation. To promote the growth of this phase we suggest an epitaxial growth on a support which provides a compressive strain. However, the presence of the cotunnite phase is undesirable in thin films used in CMOS gates. In these circumstances we recommend to grow thin films under tensile strain.

To provide a qualitative explanation of differences among the polymorphs of ZrO_2 and HfO_2, we have determined optimal atomic radii and resulting atomic charges for each species according to the procedure outlined in Sec. II above, and present them in Table V, where several trends are evident. The ionicity decreases from the monoclinic to the cotunnite phase as the volume per formula unit decreases, as evidenced by the decreasing oxygen radius relative to the metal atom, and especially from the decrease in the magnitudes of the atomic charges, moving progressively away from their formal ionic valences of +4 and −2 as we move towards the highest-pressure phase (cotunnite). However, the character of the bonding remains predominantly ionic. The population analysis results also confirm that the radii for hafnium are systematically smaller than for zirconium, a result of the

TABLE V. The effective atomic radii and pseudocharges determined at GGA minimum energy structures. Where two crystallographically distinct O atoms are present, they have been averaged.

		Monoclinic	Orthorhombic-I	Tetragonal	Cubic	Cotunnite
ZrO$_2$	r_{Zr} (Å)	0.91	0.94	1.01	0.96	1.08
	q_{Zr}	+3.50	+3.44	+3.31	+3.40	+3.11
	r_O (Å)	1.58	1.55	1.52	1.53	1.45
	q_O	−1.65	−1.61	−1.54	−1.58	−1.44
HfO$_2$	r_{Hf} (Å)	0.89	0.90	1.06	0.95	1.04
	q_{Hf}	+3.60	+3.56	+3.33	+3.49	+3.28
	r_O (Å)	1.56	1.52	1.51	1.51	1.44
	q_O	−1.69	−1.66	−1.54	−1.62	−1.49

"lanthanide contraction," whereas for a given phase the oxygen radius is very similar in HfO$_2$ and ZrO$_2$. Thus, the differences in the values of V_0 for the same polymorphs of ZrO$_2$ and HfO$_2$, which were presented in Tables II and III, derive primarily from differences in the metallic but not oxygen radii. The decrease in ionicity with compression probably results from the electron density becoming more uniform in order to minimize its kinetic energy. This increased uniformity was pointed out in Ref. 10 to make gradient corrections smaller for the high-pressure phases than for the low-pressure phases, thus explaining the differences between the LDA and GGA predictions for HfO$_2$. That explanation naturally also applies to ZrO$_2$.

Because of the omission of densities in interstitial regions when we calculate individual atomic charges, these charges do not add exactly to zero, as already noted. This "missing" interstitial charge does not exceed 0.3 electron per formula unit and increases from the low- to the high-pressure phases, consistent with the more uniform charge density in the latter.[34]

HfO$_2$ is always slightly more ionic than ZrO$_2$ in the same structure, according to the atomic charges in Table V. The effective oxygen charges are more negative in HfO$_2$ than in ZrO$_2$ and these differences result primarily from differences in the total electron density distribution, as oxygen's effective radius is very similar in both oxides. The more ionic character of HfO$_2$ vs ZrO$_2$ is consistent with slightly different electronegativities for Zr (1.4) and Hf (1.3) according to Pauling's scale.[35]

The densities of states (DOS) for five structures of ZrO$_2$ and HfO$_2$, see Fig. 4, are characterized by three parameters: (i) the width of the upper valence band, (ii) the band gap, and (iii) the width of the lower conduction band, see Table VI.

The upper valence band is dominated by oxygen $2p$ levels and its width increases from the monoclinic to cotunnite phases, i.e., as average near-neighbor interatomic distances decrease. The width is always larger for HfO$_2$ than for ZrO$_2$ (by 0.6 eV for monoclinic and 0.4 eV for cotunnite). These differences may be related to a larger concentration of electron density on oxygen atoms in HfO$_2$ than in ZrO$_2$, see Table V. The band gaps are notoriously too small in DFT calculations, but their relative values for different phases and materials are usually meaningful. The calculated band gaps for zirconia and hafnia increase from the monoclinic to the

tetragonal phase and then decrease to the cotunnite phase. The band gap is always larger for HfO$_2$ than for ZrO$_2$ (by 0.60 eV for monoclinic and 0.55 eV for cotunnite), which may be related to the difference in ionicity of these materials. Such a difference has not been yet experimentally detected with the measured value being about 6 eV for both oxides.[36] The first conduction band has mostly metal d character for each phase. For the monoclinic and orthorhombic-I phase the width of this band is broadened by crystal field effects at the
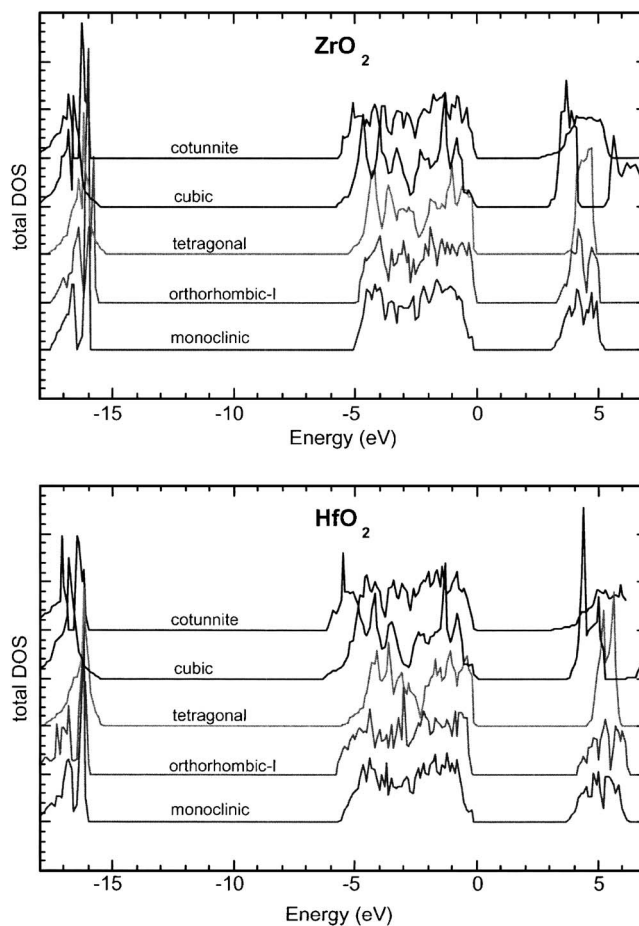
FIG. 4. The total density of states within the generalized-gradient approximation for (a) ZrO$_2$ and (b) HfO$_2$ for the five structures indicated.

TABLE VI. The width of the upper valence band (WUVB), the band gap (BG), and the width of the lower conduction band (WLCB) for different phases of ZrO_2 and HfO_2 in eV.

		WUVB	BG	WLCB
Monoclinic	ZrO_2	5.05	3.20	2.05
	HfO_2	5.65	3.80	2.55
Orthorhombic-I	ZrO_2	4.90	3.40	1.70
	HfO_2	5.60	4.30	2.15
Tetragonal	ZrO_2	5.25	3.55	1.40
	HfO_2	5.45	4.45	1.55
Cubic	ZrO_2	5.70	2.95	1.30
	HfO_2	6.30	3.70	1.55
Cotunnite	ZrO_2	5.70	2.60	2.95
	HfO_2	6.10	3.15	3.20

relatively low-symmetry metal sites. Symmetry increases for the cubic and tetragonal metal sites, fewer crystal field lines develop, and the bands are narrower. Finally, for the cotunnite phase the *d* bands are broadened again by reduced symmetry and by increased interatomic overlaps as the interatomic distances are the smallest for this phase.

The calculated heat of formation from elements (elemental solid and O_2 gas) is larger for HfO_2 (12.31 eV) than for ZrO_2 (11.71 eV) and the difference of 0.60 eV is in good agreement with the experimental difference of 0.49 eV.[8] This difference in heats of formation can contribute to a larger chemical stability of hafnia than zirconia in interfaces with other materials.[1,3]

IV. SUMMARY

We have presented density functional calculations of the total energies and equations of state of the monoclinic, tetragonal, cubic, orthorhombic-I (*Pbca*), and orthorhombic-II (cotunnite) structure phases of zirconia and hafnia in the local density (LDA) and generalized-gradient (GGA) approximations. We have confirmed the sequence of predicted low temperature phase transitions under pressure for both ZrO_2 and HfO_2 (monoclinic→orthorhombic-I→cotunnite) and our predictions are consistent with the experiment. We have also confirmed that use of the GGA is important in obtaining the correct order of phases in that the LDA predictions may be qualitatively wrong. The GGA computed transition pressures are reasonably consistent with experimental data.

The GGA value of the bulk modulus for the monoclinic phase of HfO_2 is 152 GPa and it is larger by 15 GPa than for

ZrO_2, while the difference is smaller for the high-pressure phases. For the cotunnite phase the GGA values of bulk modulus for ZrO_2 and HfO_2 are 251 and 259 GPa, respectively, whereas the respective LDA predictions are 298 and 312 GPa. Our results raise some concerns about whether cotunnite-phase ZrO_2 and HfO_2 are really "superhard" as our results are systematically smaller than the values above 400 GPa reported from some experiments.[20,21]

We developed a population analysis scheme, applicable to typical density functional theory codes for periodic systems, in which atomic radii are adapted to the actual total charge distribution in the material. The results indicate that effective atomic radius of Hf is smaller than that of Zr and the differences can be as large as 0.05 Å. This is a manifestation of the relativistic lanthanide contraction. The smaller effective size of Hf is intriguing because the main quantum number is larger for atomic Hf than for Zr.

Our population analysis provides insight into relative ionicity of different materials and their polymorphs. The ionicity decreases from the monoclinic to cotunnite phase. HfO_2 is found to be always slightly more ionic than ZrO_2 in the same structure. The more ionic character of HfO_2 vs ZrO_2 is consistent with slightly different electronegativities for Zr (1.4) and Hf (1.3) according to Pauling's scale.[35]

The calculated densities of states expose further differences between ZrO_2 and HfO_2 and their polymorphs. HfO_2 has systematically a larger width of the valence band, band gap, and width of the lower conduction band than ZrO_2. For the most common low-temperature low-pressure phases, i.e., monoclinic and tetragonal, the band gaps of HfO_2 and ZrO_2 differ by 0.6 and 0.9 eV, respectively. The lower conduction band is dominated by metal *d* states and its width is sensitive to the crystal field effects that depend upon interatomic distances and symmetry.

The calculated heat of formation from elements (elemental solid and O_2 gas) is larger for HfO_2 (12.31 eV) than for ZrO_2 (11.71 eV). This difference in heats of formation can contribute to a larger chemical stability of hafnia than zirconia in interfaces with other materials.[1,3]

*E-mail address: maciej.gutowski@pnl.gov

[1] G. D. Wilk, R. M. Wallace, and J. M. Anthony, Appl. Phys. (N.Y.) **89**, 5243 (2001).

[2] R. M. Wallace and G. Wilk, Mater. Res. Bull. **27**, 186 (2002).

[3] M. Gutowski, J. E. Jaffe, C-L. Liu, M. Stoker, R. I. Hegde, R. S.

Rai, and P. J. Tobin, Appl. Phys. Lett. **80**, 1897 (2002).

[4] L. G. Liu, Earth Planet. Sci. Lett. **44**, 390 (1979).

[5] J. Haines, J. M. Leger, and A. Atouf, J. Am. Ceram. Soc. **78**, 445 (1995).

[6] J. E. Lowther, MRS Bull. **28**, 189 (2003).

[7] F. A. Cotton, G. Wilkinson, C. A. Murillo, and M. Bochmann, *Advanced Inorganic Chemistry* (John Wiley & Sons, Inc., New York, 1999).

[8] I. Barin, *Thermochemical Data of Pure Substances*, 3rd Ed., (VCH, Wienheim, 1995), Vol. I and Vol. II.

[9] M. Copel, M. Gribelyuk, and E. Gusev, Appl. Phys. Lett. **76**, 436 (2000).

[10] J. Kang, E.-C. Lee, and K. J. Chang, Phys. Rev. B **68**, 054106 (2003).

[11] J. E. Lowther, J. K. Dewhurst, J. M. Leger, and J. Haines, Phys. Rev. B **60**, 14485 (1999).

[12] Y. Wang and J. P. Perdew, Phys. Rev. B **43**, 8911 (1991); **44**, 13298 (1991); J. P. Perdew, in *Electronic Structure of Solids '91*, edited by P. Ziesche and H. Eschrig (Akademie Verlag, Berlin, 1991).

[13] G. Kresse and J. Hafner, Phys. Rev. B **47**, R558 (1993); **48**, 13115 (1993); **49**, 14251 (1994); J. Phys.: Condens. Matter **6**, 8245 (1994); G. Kresse and J. Furthmüller, Comput. Mater. Sci. **6**, 15 (1996); Phys. Rev. B **54**, 11169 (1996).

[14] D. Vanderbilt, Phys. Rev. B **41**, R7892 (1990).

[15] M. P. Teter, M. C. Payne, and D. C. Allan, Phys. Rev. B **40**, 12255 (1989).

[16] H. J. Monkhorst and J. D. Pack, Phys. Rev. B **13**, 5188 (1976).

[17] F. D. Murnaghan, Proc. Natl. Acad. Sci. U.S.A. **30**, 244 (1944).

[18] C. J. Howard, R. J. Hill, and B. E. Reichert, Acta Crystallogr., Sect. B: Struct. Sci. **44**, 116 (1988).

[19] J. Haines, J. M. Léger, S. Hull, J. P. Petitet, A. S. Pereira, C. A. Perottoni, and J. A. H. da Jornada, J. Am. Ceram. Soc. **80**, 1910 (1997).

[20] S. Desgreniers and K. Lagarec, Phys. Rev. B **59**, 8467 (1999).

[21] J. M. Leger, A. Atouf, P. E. Tomaszewski, and A. S. Pereira, Phys. Rev. B **48**, 93 (1993).

[22] R. Ackerman, E. G. Rauh, and C. A. Alexander, High. Temp. Sci. **7**, 304 (1975).

[23] B. Králik, E. K. Chang, and S. G. Louie, Phys. Rev. B **57**, 7027 (1998).

[24] J. P. Perdew, J. A. Chevary, S. H. Vosko, K. A. Jackson, M. R. Pederson, D. J. Singh, and C. Fiolhais, Phys. Rev. B **46**, 6671 (1992); J. E. Jaffe, J. A. Snyder, Z. Lin, and A. C. Hess, Phys. Rev. B **62**, 1660 (2000).

[25] R. Orlando, C. Pisani, C. Roetti, and E. Stefanovich, Phys. Rev. B **45**, 592 (1992).

[26] X. Zhao and D. Vanderbilt, Phys. Rev. B **65**, 075105 (2002).

[27] A. S. Foster, V. B. Sulimov, F. Lopez Gejo, A. L. Shluger, and R. M. Nieminen, Phys. Rev. B **64**, 224108 (2001).

[28] A. A. Demkov, Phys. Status Solidi B **226**, 57 (2001).

[29] X. Zhao and D. Vanderbilt, Phys. Rev. B **65**, 233106 (2002).

[30] A. S. Foster, F. Lopez Gejo, A. L. Shluger, and R. M. Nieminen, Phys. Rev. B **65**, 174117 (2002).

[31] "Expressions for the Murnaghan form of $E(V)$ and $H(p)$" are reproduced in J. E. Jaffe and A. C. Hess, Phys. Rev. B **48**, 7903 (1993).

[32] O. Ohtaka, H. Fukui, K. Funakoshi, W. Utsumi, T. Irifune, and T. Kikegawa, High Press. Res. **22**, 221 (2002).

[33] A. Jayaraman, S. Y. Wang, S. K. Sharma, and L. C. Ming, Phys. Rev. B **48**, 9205 (1993).

[34] R. A. Bachorz, I. N. Yakovkin, J. E. Jaffe, and M. Gutowski, 7th Annual Meeting of the Northwest Section of APS, Victoria, BC, Canada, May 13–14, 2005 (unpublished).

[35] L. Pauling, *The Nature of the Chemical Bond* (Cornell University Press, New York, 1960).

[36] J. Robertson, MRS Bull. **27**, 217 (2002).